Numerical Simulation of Laminar Separation-Bubble Control

U. Rist, K. Augustin, S. Wagner
Universität Stuttgart, Institut für Aerodynamik und Gasdynamik
Pfaffenwaldring 21, D-70550 Stuttgart, Germany

Summary

In the present paper an active control mechanism for the control of laminar separation bubbles on airfoils is investigated by means of direct numerical simulation and linear stability theory. Boundary layer instabilities excited by periodic oscillations are utilized to control the size and length of the separation bubble and to make it finally disappear when desired. Unlike traditional vortex generators a sensor-actuator system based on this method will be adaptive to the respective flow conditions and will cause no additional undesired drag.

Introduction

Operated in a low Reynolds number regime the drag characteristics of laminar airfoils at "off-design" conditions can be considerably deteriorated by *laminar separation bubbles (LSB)*. The LSBs form due to the inability of the laminar boundary layer to overcome the stronger adverse pressure gradient caused for example by a higher angle of attack or a deflected trailing edge flap. Such an effect is shown in figure 1 by the polars c_L/c_D of a laminar airfoil at two different Reynolds numbers Re.

At $Re = 0.7 \cdot 10^6$ (low speed) with an extended flap the laminar boundary layer separates from the lower side of the airfoil just upstream of the flap. Laminar-turbulent transition occurs subsequently and the turbulent boundary layer reattaches at the rear end of the airfoil, thus forming a laminar separation bubble. The reattachment results from the increased momentum transfer towards the wall within the turbulent boundary layer. This laminar separation bubble can be removed by mounting of vortex generators upstream of the bubble which force the boundary layer into turbulence and therefore reduce the drag coefficient c_D accordingly (dashed line with diamonds). In contrast to the low speed case the properties of the airfoil at high speed ($Re = 2.5 \cdot 10^6$) and no extended flap are vice versa. The laminar boundary layer is able to overcome the pressure gradient and is not separating (solid line with squares). Vortex generators in this case produce undesired additional drag (dashed line with squares) by shortening the length of the laminar boundary on the lower side.

To obtain an adaptive vortex generator with respect to the present flow conditions we suggest to use controlled excitation of boundary layer perturbations upstream of the bubble. These disturbance waves become amplified by instability mechanisms within the laminar boundary layer and in the separation bubble itself which leads to an upstream shift of the transition and the now turbulent boundary layer does not separate. As a constraint, the upstream shifting should be achieved by a minimum of disturbance amplitude A_0 respectively of disturbance energy introduced into the flow. But the necessary amplitude A_0 can only be minimized by choosing the proper wavelength λ_x, frequency β and of course the location and length of the disturbance strip exciting sinusoidal disturbance waves.

An indicator for the effectiveness of this control is the location of transition within the LSB as shown in figure 2 where “S”, “T” and “R” mark separation, transition and reattachment, respectively. The physical investigation of the laminar separation bubble phenomenon by means of direct numerical simulation (DNS) and linear stability theory (LST) is used to estimate a control method capable to avoid separation in the “off-design” case without deteriorating the design properties of the airfoil.

Based on the considered method an actuator-sensor concept will be designed, where the LSB is detected by sensors and an upstream actuator driven by a controller (figure 3) excites the boundary layer disturbances.

Numerical method

The implemented 3D DNS method [1] solves the complete Navier-Stokes equations for incompressible flow in a vorticity-velocity formulation

$$\frac{\partial \underline{\omega}}{\partial t} - \mathrm{rot}\,(\underline{v} \times \underline{\omega}) = \frac{1}{Re}\,\Delta\underline{\omega} \qquad (1)$$
$$\text{with} \quad \underline{v} = (u,v,w) \quad \text{and} \quad \underline{\omega} = (\omega_x,\omega_y,\omega_z)$$

within a rectangular integration domain (A-B-C-D in figure 2) over a flat plate.

All spatial coordinates are non-dimensionalized by a reference length $\tilde{L}$ and velocities by the free-stream velocity $\tilde{U}_\infty$, where $\tilde{}$ denotes dimensional variables. This leads, together with the kinematic viscosity $\tilde{\nu}$, to the following definitions for the vorticity vector $\underline{\omega}$ and the frequency β

$$\underline{\omega} = -\,\mathrm{rot}\,\underline{v}\,, \quad \beta = \frac{2\pi\,\tilde{f}\,\tilde{\nu}}{\tilde{U}_\infty} \cdot 10^5\,, \quad \mathrm{Re} = \frac{\tilde{U}_\infty \tilde{L}}{\tilde{\nu}}. \qquad (2)$$

Fourth-order accurate finite differences are used on the equidistant numerical grid in streamwise (x-) and wall-normal (y-) direction whereas a spectral Fourier ansatz in spanwise (z-) direction is applied. The explicit time integration is realized by a fourth order, four step Runge-Kutta scheme. Once the three vorticity components are obtained, three Poisson equations for the remaining velocities u, v and w have to be computed. Due to the spectral ansatz in spanwise direction the Poisson equations for the u and v velocity reduce to ordinary differential equations (ODE) and only the v-equation has to be solved iteratively by a line relaxation method accelerated by a multigrid scheme [7].

At the inflow boundary steady Falkner-Skan or, at zero pressure gradient, Blasius velocity profiles are prescribed. In a relaminarization zone [2] upstream of the outflow boundary the unsteady vorticity components are damped to steady state values to avoid non-physical reflections and as a consequence the unsteady velocity components $\underline{v}'$ vanish exponentially. At the wall the no-slip condition is applied except for a disturbance strip where 2D and 3D perturbations can be introduced into the flow by periodic suction and blowing.

To take into account the strong boundary layer displacement effects of the LSB a viscous-inviscid interaction model is implemented into the multigrid algorithm for the v-velocity component. At run time a velocity distribution which allows for the typical boundary layer displacement effects of a LSB evolves from the initially prescribed potential flow. For a detailed summary of the interaction model and boundary conditions refer to [3]. Figure 4 shows the initial potential distribution of the u-velocity (dashed line) and the resultant distribution considering the effects of the LSB (solid line).

Once the DNS has yielded a reasonable mean flow the development of excited boundary layer perturbations can be studied with less effort by using the linear stability theory (LST) [8]. However, the LST can provide correct results in the linear regime of the disturbance development only, i.e. upstream of transition ("T") and cannot cover variations of the mean flow due to the strong influence of different disturbance amplitudes A_0 on the size of the LSB. Applying the LST the spatial amplification rate α_i of discrete fluctuations specified by their streamwise wavenumber α_r and disturbance frequency β in

$$v(x, y, t) = \Re\left\{\hat{V}(y)\ e^{i(\alpha x - \beta t)}\right\} \quad \text{with} \quad \alpha = \alpha_r + i\,\alpha_i \tag{3}$$

can be determined by solving the Orr-Sommerfeld equation. Values of $\alpha_i < 0$ mean amplification and $\alpha_i > 0$ damping of the disturbance amplitude. The disturbance amplitude $A(x)$ can thereon be obtained by integrating the amplification rate α_i in streamwise x-direction and multiplying these values with an initial disturbance amplitude A_0.

Control of LSB by boundary layer disturbances

The present quantitative investigations are performed for a pressure-induced LSB in a flat-plate boundary layer where a Blasius boundary layer solution with $Re_{\delta_1} = 1722$ is prescribed at inflow and a streamwise velocity deceleration by 10% is prescribed at the free stream boundary (cf. figure 4). The other parameters of the flow are Re=100000 (for $x = 1$), $\Delta x = 0.008376$, $\Delta y = 0.002296$, and $\Delta t = 0.002513$. This case is comparable to the "midchord-bubble" considered in greater detail in [6].

Comparing the amplification curves $u'_{max}(y)/U_\infty$ for the fundamental disturbance mode with $\beta = 5.0$ in figure 5 yields an excellent agreement between LST and DNS. This is illustrated in the $A_v = 10^{-6}$ case (dash-dotted and dash-dotted line with squares), where A_v is the amplitude of the wall-normal velocity disturbance within the disturbance strip at the wall. Both curves evidently coincide which shows that the LST is able to predict the disturbance development in flows with LSB once the flow field has been computed.

The amplification curves in figure 5 clearly show an upstream shift of the point of amplitude saturation with increasing A_v which coincides with transition. It can be expected that this upstream shift will reduce the size of the LSB.

This influence on the size of the bubble is also present in the local mean velocity profiles of the streamwise velocity u at certain x-positions. In figure 6 the velocity profiles at the point of separation a) and at the point of reattachment b) of the case $A_v = 10^{-4}$ (with the smallest LSB) are shown for comparison with the other considered cases. The reference case without disturbance excitation shows the greatest differences. The boundary layer has separated upstream and is still separated in b) where a fully developed separation profile with reverse flow ($u < 0$) close to the wall is visible. All other cases show the same properties at these positions but with higher disturbance levels the size and the strength of the region of reverse flow becomes smaller and smaller and together with it the overall size of the LSB reduces.

This strong influence of even very small disturbances ($A_v \ll 1$) on the shape and the size of the time averaged separation bubble is displayed in figure 7. On the left hand side by streamlines including the separation line (emphasized) versus the streamwise coordinate x and on the right hand side by the mean skin friction distribution ω_{zw} for the five cases $A_v = 0$ to $A_v = 10^{-4}$ already considered in the preceding figures.

The large separation bubble which contains a large recirculation vortex at its rear end is reduced in size. Only a very small bubble is visible at a disturbance level of $A_v = 10^{-4}$ and no recirculation vortex. Moreover, the strong displacement of the boundary layer by the large separation bubble, which would affect the pressure distribution of an airfoil and cause additional drag, almost vanishes with an increased disturbance level. Both the separation and reattachment point are shifted leading to a reduction of the bubble in size. The reattachment point is shifted upstream by the growing influence of the disturbance excitation and the thereby earlier transition. In addition to that the separation point moves further downstream towards the reattachment because of upstream effects of the transition location on the wall-pressure (cf. [6]). In other words, the bubble becomes shallower with increased forcing and exerts less displacement on the potential flow.

The LSB can be detected by the negative values of the time averaged (in this case over two disturbance cycles) skin-friction distribution ω_{zw} in the right-hand-side figures. The streamwise length of the bubble is marked by arrows. The initially only small negative values of ω_{zw} turn into strong skin friction at the rear end of the bubble with a small region of positive values in between. This region is the footprint of the recirculation vortex at the end of the bubble whose strength weakens with increasing disturbance amplitude. High positive values of the skin friction ω_{zw} downstream of the bubble are caused by the large-amplitude (saturated) disturbances that mimic a turbulent boundary layer in the present computations.

Therefore, the skin friction can be used to sense the occurrence of a LSB. Different shear stress sensors for this purpose are currently under development, for example in [5], but not yet available.

Based on the present results a controlling mechanism (cf. figure 3) consisting of an oscillating piezoceramics actuator, which has already been built and tested [4], will be derived. For the present design the oscillation frequency signal for the actuator is provided by a signal generator and only the amplitude A_v will be controlled. An estimation of suitable dimensional disturbance frequencies $\tilde{f}$ for maximum amplification is quoted in table 1 with respect to different free-stream velocities $\tilde{U}_\infty$.

Table 1 Estimation of required dimensional frequencies $\tilde{f}$ with respect to the free stream velocity $\tilde{U}_\infty$.

$\tilde{U}_\infty$	$\frac{m}{s}$	20	30	40	50
$\tilde{f}$	Hz	425	955	1700	2650

The already tested actuator showed the capability of a maximum frequency of more than 1 kHz and a maximum amplitude of the surface deformation of several μm. The controller will read the signal from the sensor and determine the size of the LSB by averaging the signal over a certain period of time, e.g. ten disturbance periods. The controller is necessary to avoid excessive disturbance amplitudes, to react on nonlinearities in the control loop, and to enable the mechanism to respond to changing flow conditions where a LSB might not be present.

Conclusion

A boundary layer flow with laminar separation bubble has been ivestigated by means of linear stability theory and direct numerical simulation. Hereon a method has been suggested that utilizes the instability mechanisms of the flow to influence the size of the separation bubble. An amplification of properly chosen disturbances can be observed up to an amplitude where an

evident change in the size of the bubble results. Further simulations are expected to lead to a sensor-actuator system based on wall shear stress sensors and a piezoceramics driven actuator. This system will be capable of generating the desired disturbances if activated when a separation bubble is about to occur. Otherwise it will not generate any additional drag.

Acknowledgments

The financial support of the Deutsche Forschungsgemeinschaft (DFG) via the Sonderforschungsbereich 409 "Adaptive Strukturen im Flugzeug- und Leichtbau" at the Universität Stuttgart is gratefully acknowledged.

References

[1] Markus Kloker. Direkte numerische Simulation des laminar-turbulenten Strömungsumschlags in einer stark verzögerten Grenzschicht. Dissertation, Universität Stuttgart, 1993.

[2] Markus Kloker, Uwe Konzelmann and Hermann F. Fasel. Outflow boundary conditions for spatial Navier-Stokes simulations of transition boundary layers. *AIAA Journal*, 31(4):620–628, April 1993.

[3] Ulrich Maucher, Ulrich Rist and Siegfried Wagner. Refined interaction method for direct numerical simulation of transition in separation bubbles. *AIAA Journal*, 38(8):1385–1393, 2000.

[4] Jörg Müller. Konzeptstudie für ein aktives Oberflächenfeld zur Verhinderung laminarer Strömungsablösung. Studienarbeit, Bereich Flugzeugentwurf, Fakultät Luft- und Raumfahrttechnik, Universität Stuttgart, September 1999.

[5] Tilmann von Papen and Ha Duong Ngo. Entwicklung eines mikromechanischen Oberflächenzauns für den Einsatz in Rückströmgebieten. In Martin Schober and Jan Schulz, editors, *Doktorandenkolloquium des SFB 557 "Beeinflussung komplexer turbulenter Strömungen"*. Hermann Föttinger Institut, TU Berlin, Oktober 1999.

[6] Ulrich Rist. Zur Instabilität und Transition in laminaren Ablöseblasen. Habilitationsschrift, Universität Stuttgart, 1998. Shaker Verlag, 1999.

[7] Ulrich Rist and Hermann F. Fasel. Direct numerical simulation of controlled transition in a flat-plate boundary layer. *J. Fluid Mech.*, 298:211–248, 1995.

[8] Hermann Schlichting. *Boundary Layer Theory*, chapter Origin of Turbulence I, pages 459–483. McGraw-Hill, 1979.

Figures

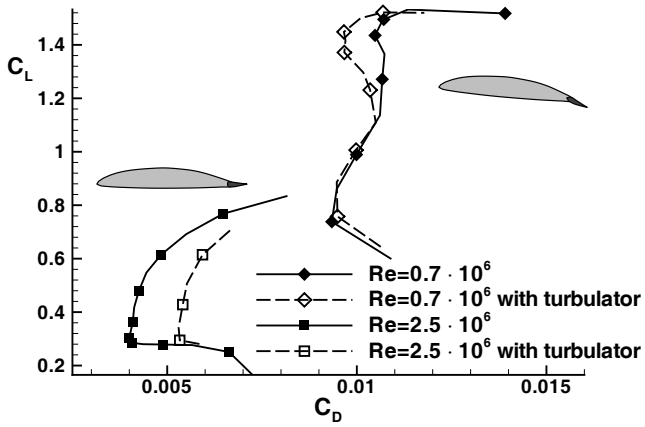

Figure 1 Lift vs. drag coefficients at two different Reynolds numbers with and without vortex generators on the lower side of a laminar airfoil.

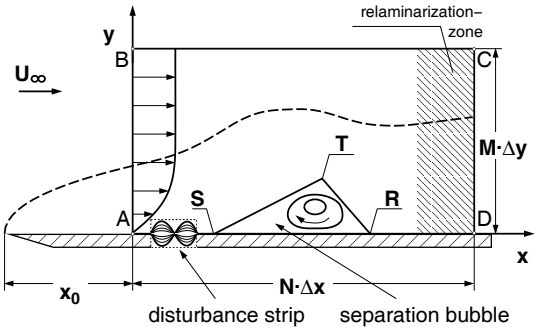

Figure 2 Schematic overview of the integration domain of the DNS with LSB.

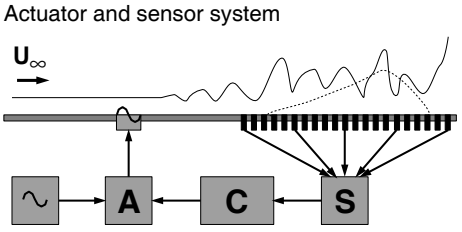

Figure 3 Sensor (S)-actuator (A) concept with controller (C) and signal generator ($\sim$).

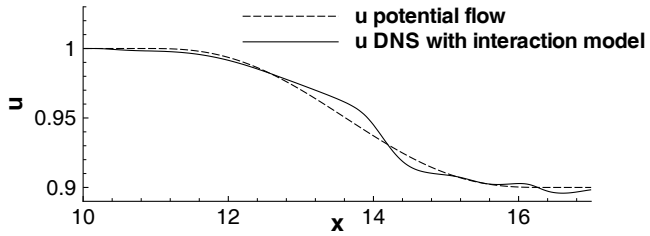

Figure 4 u-velocity distribution at the free-stream boundary.

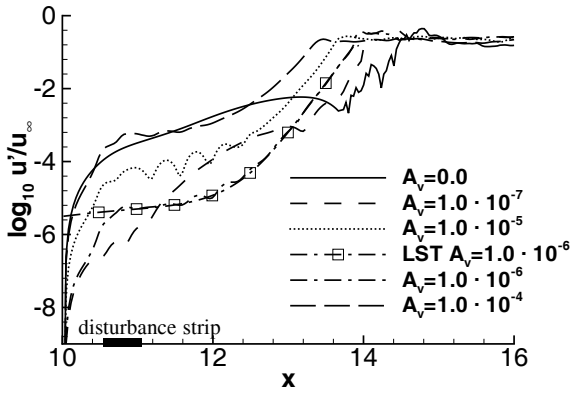

Figure 5 Amplification curves as a result of DNS and LST at different levels A_v of excited boundary layer perturbations with frequency $\beta = 5$.

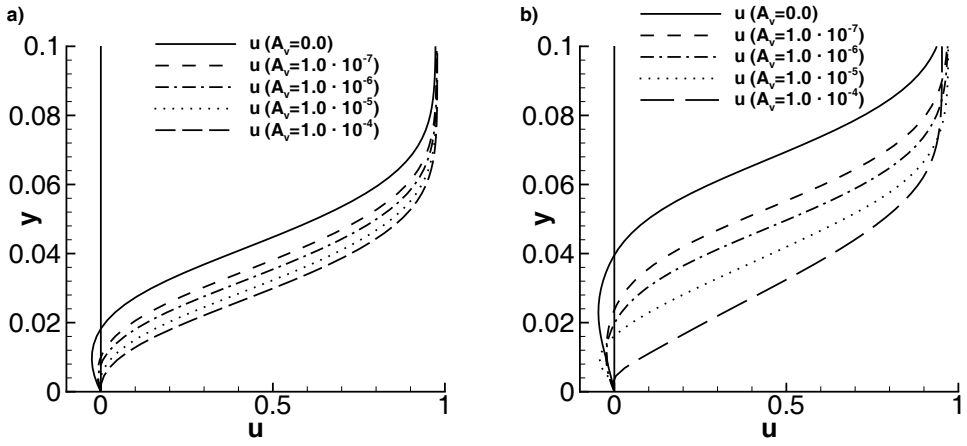

Figure 6 Wall normal distribution of the streamwise time-averaged velocity u at a) separation of the $A_v = 10^{-4}$ case and b) reattachment of the $A_v = 10^{-4}$ case.

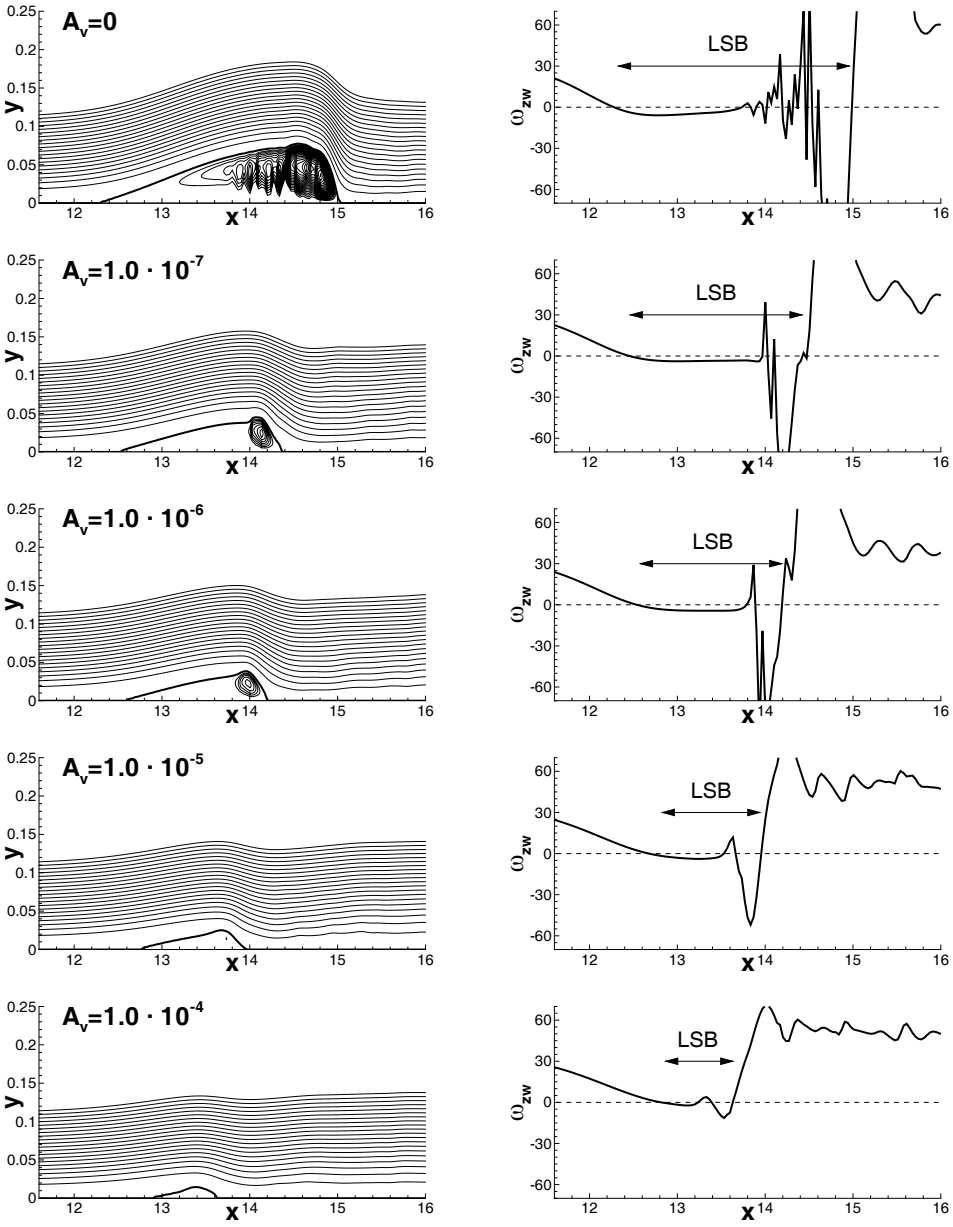

Figure 7 Streamlines and separation line of the time-averaged flow with separation bubble and corresponding skin friction distribution ω_{zw}.